Nanoscale

PAPER

View Article Online
View Journal | View Issue

Cite this: *Nanoscale*, 2014, **6**, 8969

Light-induced reversible modification of the work function of a new perfluorinated biphenyl azobenzene chemisorbed on Au (111)†

Appan Merari Masillamani,[a] Silvio Osella,[b] Andrea Liscio,[c] Oliver Fenwick,[a] Federica Reinders,[d] Marcel Mayor,*[de] Vincenzo Palermo,*[c] Jérôme Cornil*[b] and Paolo Samorì*[a]

Received 7th April 2014
Accepted 5th June 2014

DOI: 10.1039/c4nr01880j

www.rsc.org/nanoscale

We describe the synthesis of a novel biphenyl azobenzene derivative exhibiting: (i) a protected thiol anchoring group in the α-position to readily form self-assembled monolayers (SAMs) on Au surfaces; and (ii) a terminal perfluorinated benzene ring in the ω-position to modify the surface properties. The design of this molecule ensured both an efficient *in situ* photoswitching between the *trans* and *cis* isomers when chemisorbed on Au(111), due to the presence of a biphenyl bridge between the thiol protected anchoring group and the azo dye, and a significant variation of the work function of the SAM in the two isomeric states, induced by the perfluorinated phenyl head group. By exploiting the light responsive nature of the chemisorbed molecules, it is possible to dynamically modify *in situ* the work function of the SAM-covered electrode, as demonstrated both experimentally and by quantum-chemical calculations, revealing changes in work function up to 220 meV. These findings are relevant for tuning the work function of metallic electrodes, and hence to dynamically modulate charge injection at metal–semiconductor interfaces for organic opto-electronic applications.

1. Introduction

Photochromes are light sensitive molecules which are capable of undergoing isomerisation between two or more (meta) stable states when exposed to external electromagnetic stimuli.[1] Among them, azobenzenes are particularly interesting since they can photoisomerise from a fully extended *trans* form to a bent *cis* form and *vice versa* when exposed to ultraviolet or visible light, respectively.[2] Azobenzenes can be equipped with anchoring groups to promote chemisorption on metallic electrodes, forming highly ordered self-assembled monolayers (SAMs).[3] The light-induced modification of azobenzene SAMs has been shown to be a successful route to reversibly modulate functional properties of surfaces and interfaces for electronic applications.[4] Properties that can be modulated in this way include the work functions of metal surfaces,[5] current density in monomolecular layers,[6] optical properties of SAMs[7] (and thin films[2b]) and charge injection in organic field-effect transistors (OFET).[8] We have recently shown that a significant variation of the work function in presence of azobenzene SAMs can be obtained by functionalisation of the molecule with a perfluorinated head group, observing that the magnitude of the switch is determined not only by changes in a molecular dipole contribution but also by the counter-acting effect of the bond dipole. The *in situ* work function variation in the prior work was slightly lower than predicted by quantum-chemical calculations (90 meV *versus* 200 meV), possibly because the short (monophenyl) anchoring group could allow electrode quenching of the excited state of the *trans* isomer before isomerisation occurs, with the consequence of a low photo-isomerization yield on the surface.[9]

In this manuscript we report the synthesis of a new perfluorinated functionalized azobenzene molecules possessing a biphenyl bridge connecting the protected thiol anchoring group and the azo moiety. We investigate the *ex situ* and on-surface (*in situ*) reversible change in the SAM work function, going from a *trans* to *cis* isomeric form and *vice versa* when exposed to UV and visible light, respectively. Such a dynamic change in the work function has been monitored experimentally at different length scales using various techniques such as photoelectron spectroscopy, macroscopic Kelvin probe and Kelvin Probe Force Microscopy (KPFM), and further corroborated by quantum-chemical calculations.

[a]*ISIS & icFRC, Université de Strasbourg & CNRS, 8 allée Gaspard Monge, 67000 Strasbourg, France. E-mail: samori@unistra.fr*

[b]*Laboratory for Chemistry of Novel Materials, University of Mons, Place du Parc 20, B-7000 Mons, Belgium. E-mail: Jerome.Cornil@umons.ac.be*

[c]*ISOF-CNR, via Gobetti 101, 40129 Bologna, Italy. E-mail: palermo@isof.cnr.it*

[d]*Department of Chemistry, University of Basel, St. Johannsring 19, 4056 Basel, Switzerland. E-mail: marcel.mayor@unibas.ch*

[e]*Karlsruhe Institute of Technology KIT, Institute for Nanotechnology, P.O. Box 3640, 76021 Karlsruhe, Germany*

† Electronic supplementary information (ESI) available: Synthetic pathway, characterisation of **1** and intermediates. See DOI: 10.1039/c4nr01880j

Note that we use the acetyl protected derivate **1** for the SAM to avoid the formation of hardly soluble disulfides, while for the theoretical studies the sulphur radical terminated derivate was considered to reduce the complexity and computing processing costs.

2. Methods

2.1 Synthesis of 1

The synthesis of the terminally fluorinated biphenyl azobenzene **1** was achieved in 5 steps and is displayed in Scheme 1. Key steps are the *Suzuki* coupling to assemble both biphenyl subunits and the *Mills* reaction for the asymmetric azo coupling. In particular, the first biphenyl synthon **4** was obtained by coupling the boronic acid ester derivative **2** with pentafluoroiodobenzene **3**. Removal of the BOC protection group in **4** gave the bipehnylamine **5**, which reacted with 1-bromo-4-nitrosobenzene to provide the azo derivative **6** in a *Mills* condensation. The bromine substituent of **6** enabled the second *Suzuki* coupling with boroxine 7 resulting in the biphenyl-azo-derivative **8**. Transprotection of the arylthiol provided the target structure **1**. Synthetic protocols and a full characterization of all compounds are provided in the ESI.† The identity of all new compounds was corroborated by ^{1}H-, ^{19}F-, and ^{13}C-NMR spectroscopy, mass spectrometry and elemental analysis.

2.2 Preparation of SAMs of 1

10 μM solutions of **1** in chloroform were prepared in a volumetric flask and stored inside the cool dark environment of a refrigerator.

To prepare SAMs in the *trans* form, ozone treated clean gold on mica (Georg Albert PVD, Germany) was immersed in the solution for 24 h in an air tight beaker. It was found that no deprotection of **1** was required to form SAMs, as has been reported in the literature for a number of thioacetate-terminated conjugated molecules[10] – though it is known that the kinetics are somewhat slower than for SAM formation from analogous thiols.[10b,11]

To prepare *ex situ* SAMs in the *cis* form, a beaker containing a solution of **1** was placed under an inverted cardboard box and irradiated through a slit with UV light at $\lambda = 366$ nm (8 W electrical power) for a period of 120 s. Subsequently, clean gold substrates were removed from the ozone treatment chamber and immediately immersed in the *cis* solution for 24 h inside a refrigerator at 4 °C. Solution absorption spectra displayed in Fig. 1d confirm that the *cis* to *trans* back reaction does not progress significantly over a period of 24 h at 4 °C.

For both the *trans* and *cis* SAMs, after 24 hours, the gold substrates were removed from the solution and rinsed with a large volume of pure chloroform solution and dried under a gentle stream of nitrogen gas.

2.3 Ambient photoelectron spectroscopy

The work function of the electrodes modified with the SAMs was measured by means of ambient photoelectron spectroscopy with a Riken Keiki spectrophotometer (Japan) model AC-2. The conditions employed during the measurements were a scanning energy range from 4.0 to 6.2 eV with a measurement interval of 0.1 eV and UV spot intensity of 10 nW.

2.4 Macroscopic Kelvin probe

The surface potential difference of the SAMs on gold was measured by means of ambient macroscopic Kelvin probe KP020 (KP Technology Ltd, UK). A gold tip of 2 mm diameter was used as the probe electrode. A sample of bare gold film on mica was used as a reference.

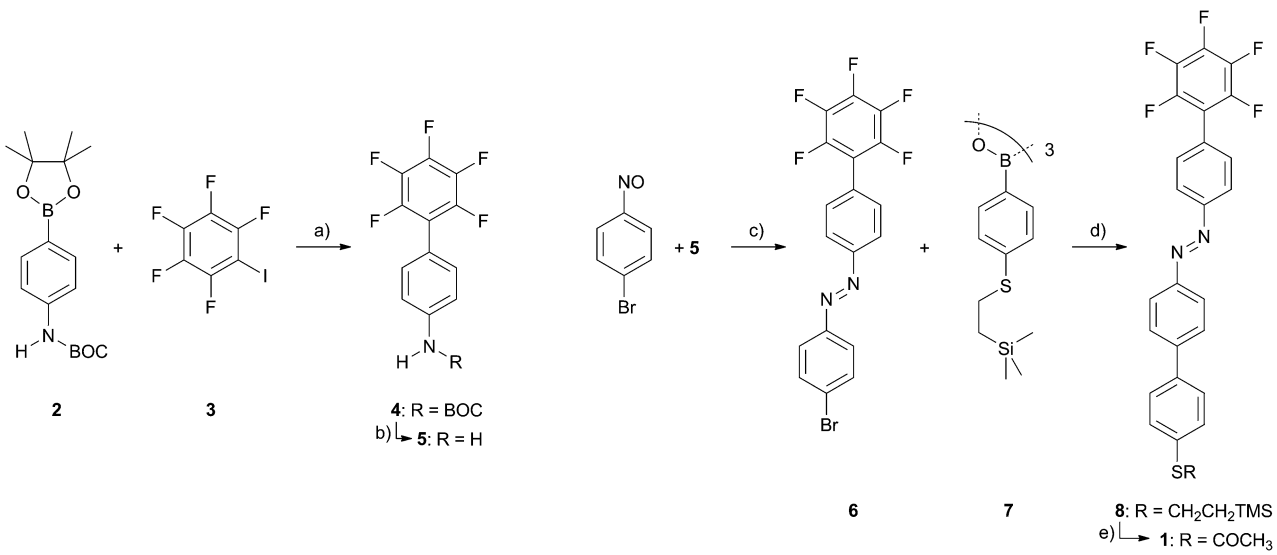

Scheme 1 Synthesis of the terminally fluorinated azo-rod **1**. Reagents and conditions: (a) $Pd(PPh_3)_4$, Cs_2CO_3, $C_6H_5CH_3$, reflux, 30 h, 60%; (b) CF_3COOH, CH_2Cl_2, reflux, 1 h, 98%; (c) 1-bromo-4-nitrosobenzene, CH_3COOH, RT, 29h, 89%; d) **7**, $Pd(PPh_3)_4$, K_2CO_3, $C_6H_5CH_3$, CH_3CH_2OH, 60 °C, 45 min, 98%; (e) CH_3COCl, $AgBF_4$, CH_2Cl_2, RT, 20 min, 83%.

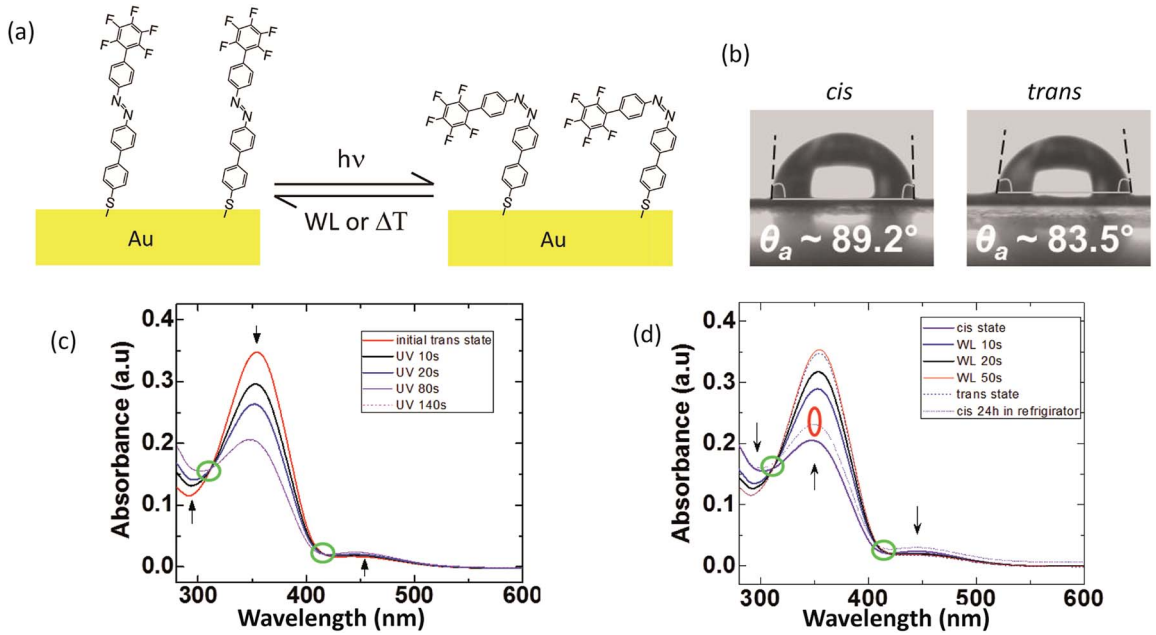

Fig. 1 (a) Schematic of a SAM of **1** shown on a gold surface in its fully extended *trans* form (left) and its *cis* form (right). (b) Water contact angle measurements of SAMs of **1** in the *trans* and *cis* forms (prepared *ex situ*). UV-vis spectrum of **1** in solution showing (c) *trans* to *cis* isomerisation under UV illumination, and (d) *cis* to *trans* isomerisation under white light illumination. The isosbestic points are indicated with green circles and the red oval shows the spectrum after 24 h cooling in a refrigerator maintained at 4° C.

2.5 Kelvin probe force microscopy

KPFM measurements were performed in air by employing a commercial microscope Multimode III (Bruker, Germany) with extender electronics module. In order to obtain a sufficiently large and detectable mechanical deflection, we used ($k = 2.8$ N m^{-1}) Pt/Ir coated Si ultra-levers (SCM-PIT, Bruker) with oscillating frequencies in the range $60 < \omega < 90$ kHz. AFM and KPFM images are acquired in the same measurement; a topographic line scan is first obtained by AFM operating in tapping mode and then that same line is rescanned in lift mode with the tip raised to a lift height of 10 nm.

KPFM technique provides a voltage resolution of about 5 mV and a lateral resolution of a few tens of nanometres. Calibration of the probe was carried out against a freshly cleaved Highly Oriented Pyrolytic Graphite (HOPG) surface.[12] Comprehensive description of the two techniques can be found in[13] and references therein.

2.6 Water contact angle

Contact angles of sessile water drops on functionalised Au(111) surfaces were measured with a Krüss DSA100 Drop Shape Analyser.

2.7 Theoretical simulations

A 2D periodic slab made of five layers of Au(111) with a lattice parameter of 4.1 Å (Au–Au distance of 2.9 Å) was built.[14] The chosen number of gold layers ensures a good convergence of the results when varying the thickness of the slab; a vacuum region of 40 Å is introduced in the third direction to avoid electrostatic interactions between repeated slabs. In order to assess exclusively the influence of the fluorination pattern in **1**, we have adopted the same unit cell as that considered for the non-fluorinated analogue on the basis of experimental STM images, with $a = 8.7$ Å; $b = 7.7$ Å, and $\alpha = 79°$ (Fig. 2a, red frame);[5b] this represents the best compromise between the limited size of the unit cell that we can treat and the gold surface periodicity constraints. Based on our findings for the previously studied compounds, we have introduced two independent chemisorbed molecules within a herringbone packing for both isomeric forms. The sulphur atom has been initially anchored in a bridge position for both isomeric forms, as suggested by our previous study on the non-fluorinated analogue.[5b] To further investigate the influence of the structure of the SAM on the calculated properties, the two non-equivalent molecules were also attached with the same intermolecular distance and bridge anchoring position but in a different starting geometry (*i.e.*, different spatial positions on the Au (111) surface). Along the line of our previous works,[5b,c] the geometry of the cells has been optimized at the density functional theory (DFT) level using the SIESTA3 package,[15] with a full relaxation of the molecule and the top two gold layers. The local density approximation (LDA) has been used in conjunction with the Ceperley–Alder exchange–correlation functional.[16] The valence electrons are described within the LCAO approximation using a DZP basis set[15] whereas Troullier–Martins pseudopotentials are used for the description of the core electrons. We use a mesh cut-off of 250 Ry and a k-sampling of (5,5,1) in the Monkhorst-Pack scheme.[17] The parameters of the DZP basis have been adapted in the same way for all atoms so that the work function of the clean gold (111) surface matches the experimental value of

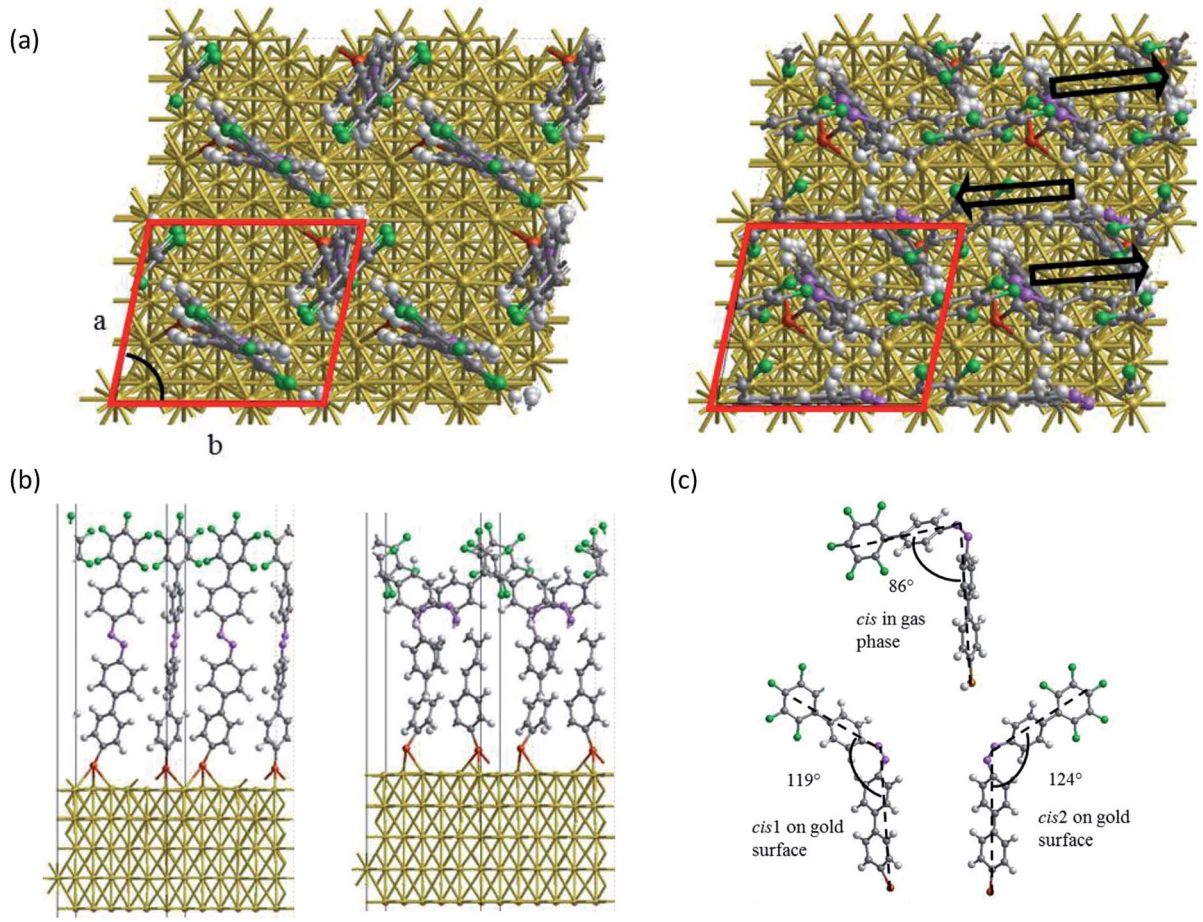

Fig. 2 (a) Optimized geometries of the unit cell for the *trans* (left) and *cis* (right) isomers (view along normal to surface). The arrows depict the opening direction of the *cis* form; the red frame is a top view of the unit cell. The parameters used are: $a = 8.7$ Å; $b = 7.7$, and $\alpha = 79°$. (b) Side views of a single unit cell for the geometries (a) for the *trans* (left) and *cis* (right) isomers. Seemingly broken bonds in the *cis* SAM occur are where the molecule crosses the unit cell borders. (c) Optimized geometry of the *cis* form in the gas phase (top) and of the two independent molecules in the unit cell on the gold surface (bottom). The colours employed for the atoms are the following: gray: carbon, white: hydrogen, purple: nitrogen, green: fluorine, red: sulphur and yellow: gold.

5.26 eV.[14] The choice of the LDA approximation is justified by the fact that in our experience, LDA and the generalized gradient approximation (GGA) give very similar work function shifts for SAMs chemisorbed on a metallic electrode for a given contact geometry; moreover, we do not expect the interface geometry to be radically different when using these two different approximations in view of the high packing density of the molecules on the surface. Since the possible degrees of freedom are strongly limited by the chemical anchoring of the molecules on the gold surface *via* the S–Au bond and by the full coverage of the metal surface, neither do we expect that the van der Waals interactions will strongly impact the present results. Note also that the herringbone packing observed for the *trans* isomer is driven by quadrupolar effects and that such electrostatic interactions are fully accounted for by the calculations.

After optimization, the sulphur atom is located on a bridge site for both isomers and both different spatial layouts, thus providing evidence that the anchoring position does not change upon isomerisation.[5b] The average SAM thickness is about 22.6 Å for the *trans* isomer and 19.1 Å for the *cis* isomer. Fig. 2a shows the optimized structure of the cell for the two isomeric forms. The *trans* isomers pack into a herringbone structure with a tilt angle of 6.4° (3.4° for the second non-equivalent molecule) between the surface normal and the vector connecting the sulphur atom and the top carbon atom. The *cis* isomer of both starting geometries exhibits an opening angle in the structure (119° and 124°) which is much larger than for the molecule in the gas phase (86°, as calculated in a large unit cell to prevent intermolecular interactions) due to increased steric effects in the SAM, Fig. 2b. The phenyl ring next to the surface is found to be slightly less tilted (with respect to the normal to the surface) on average for the *trans* isomer of both starting geometries (13.3° and 6.9° for the two independent molecules) than for the *cis* isomer (17.3° and 7.6°). In spite of the steric hindrance induced by the fluorine atoms on the last phenyl ring, the tilt angle for the *trans* isomer and the opening angle of the *cis* isomer are very close to the values calculated for the non-fluorinated azobenzene derivative (7.2° and 117°, respectively). The same holds true for the angle between the surface normal and the first phenyl ring of the molecule (*cis*: 16.1° and 7.1°; *trans*: 13.1° and 6.8°).

The electronic density calculated at the equilibrium geometry can be exploited to plot the plane averaged electrostatic potential along the axis normal to the interface; this provides a direct estimate of the work function shift by comparing the converged potential on the bare side of the surface and on the SAM-covered side of the surface. The total work function shift ($\Delta\Phi$) can also be reduced into a molecular contribution (ΔV_{SAM}) arising from the dipole supported by the molecular backbone and a bond dipole (BD) contribution describing the interfacial electronic reorganization upon formation of the Au–S bond.[18]

$$\Delta\Phi = \Delta V_{SAM} + BD \quad (1)$$

The magnitude of these two contributions depends whether we are considering that radicals or neutral molecules approach the gold surface to make a covalent Au–S bond; the radical scenario has been used here for sake of consistency with our previous studies.[19] ΔV_{SAM} has been estimated here by computing at the spin polarized LDA level the electrostatic potential profile across a sheet of radicals obtained by removing the metal surface from the full system while keeping the same geometry for the molecular part. The value of BD is then obtained by subtracting ΔV_{SAM} from $\Delta\Phi$ since we do not expect major surface restructuration of the gold surface.[20] It is worth stressing that the nature of the terminal group (thiol *versus* thioacetate) is not relevant when computing the work function shifts. Indeed, the terminal hydrogen atom of the thiol group or the acetate part are eliminated upon chemisorption. Since the theoretical analysis has been made here in a radical scenario, the nature of the actual terminal units does not change the results.

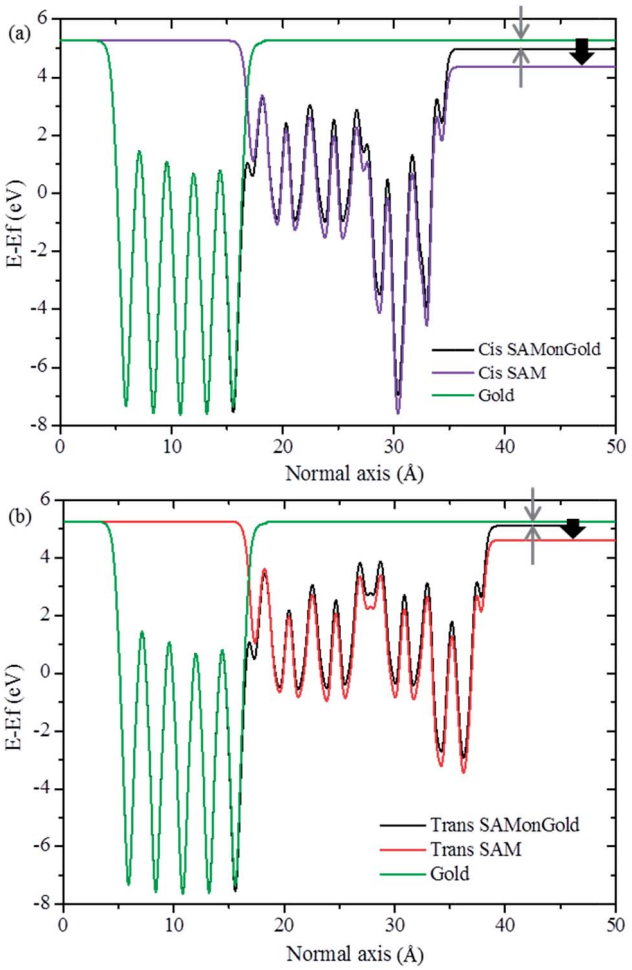

Fig. 3 Plane averaged potentials of the (a) *cis* and (b) *trans* isomer on the gold (111) surface. We display curves for the bare Au(111) surface (green), the gold surface covered by the SAM (black), and the free SAM layer (purple and red for the *cis* and *trans* isomer, respectively). In the left part, we can identify the five gold layers and the SAM contribution moving away from the surface. The arrows on the right side points to the work function shift of the full system (light gray) and to the contribution arising from the free SAM (black arrow). The difference between these shifts corresponds to the bond dipole.

3. Results and discussions

3.1 Theoretical considerations

Fig. 3 shows the calculated plane averaged potential profiles associated with the optimized structures of the unit cell for the *trans* and *cis* isomers. The computed work function of the Au(111) surface modified with the *trans* and *cis* isomers amount to 5.10 eV and 4.96 eV, respectively; this represents a decrease by −0.15 eV and −0.29 eV with respect to the clean metal surface. The higher work function observed for the *trans* form is fully consistent with the experimental data (*vide infra*), leading to a final difference between *trans* and *cis* forms ($\Delta_{CT}\Phi$) of 140 meV. Similar results were obtained when considering a different initial layout for the two isomers.

In order to investigate the contributions to this shift of the bond dipole *versus* the dipole supported by the molecular backbone, the computed potential profile of the free SAM is shown in Fig. 3. For the *trans* form, the molecular contribution is −0.68 eV, leading to a bond dipole of +0.53 eV. A much higher value of −0.95 eV is obtained for the *cis* form, which translates into a bond dipole of about +0.66 eV. The shift of the work function is thus driven by two counter-acting contributions.

The evolution of the generated bond dipole when moving from the left side to right side of the system is plotted in Fig. 4 for both isomers as well as the computed difference between *cis* and *trans* isomers. This difference is zero on the left side and it amounts to a total value of 130 meV on the right side (0.66–0.53 eV). This graph illustrates that the bond dipole significantly grows in between the sulphur atom and the first nitrogen atom for both isomers. The bond dipole difference between *cis* and *trans* forms is about 56 meV near the sulphur atom to be compared with the final difference of 130 meV.

The contribution of the molecular backbone to $\Delta\Phi$ arises from its dipole moment. For the *cis* isomer, the dipole moment of the radical evolves from 4.46 D in the gas-phase optimized geometry (as calculated in a large unit cell to avoid intermolecular interactions) to 4.65 D and 4.01 D for the isolated radical molecules adopting the structure of the non-equivalent units in the SAM; the dipole slightly changes for the *trans* isomer from 2.69 D to 2.78 D and 2.61 D, respectively. Depolarization effects then come into play to modify these individual dipoles when

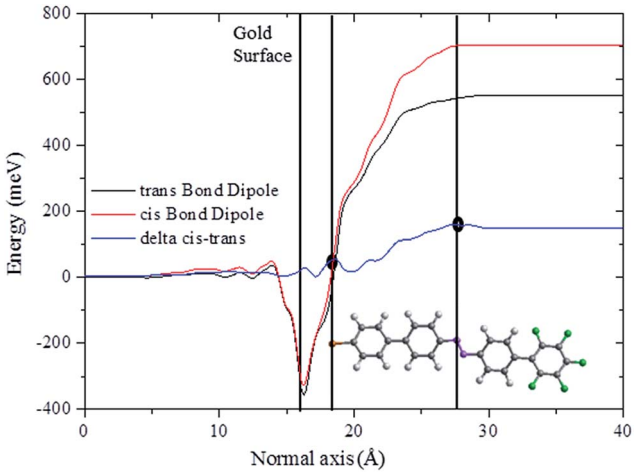

Fig. 4 Evolution of the bond dipole at the metal/SAM interface from the left to the right side. The black and red lines correspond to the *trans* and *cis* isomers, respectively. Reference vertical lines correspond to the gold surface and different positions along the molecular backbone in the superimposed *trans* geometry. The bond dipole first decreases in the vicinity of the Au–S bond due to the repulsion of the electronic cloud of gold at the surface by the atoms of the deposited molecule (*i.e.*, pillow effect), then steadily grows to reach its final value. The blue line corresponds to the difference between the bond dipoles of the two isomers.

accounting first for the intermolecular interactions between the two non-equivalent molecules within the SAM.[21] The total dipole of the two non-equivalent radical molecules is 7.82 D for *cis* and 4.90 D for *trans*, thus showing a small depolarization of about 10% compared to the isolated molecules (4.65 + 4.01 = 8.66 D for *cis* and 2.78 + 2.61 = 5.39 D for *trans*). The use of periodic conditions further reduce the dipole of the cell by up to 80%, leading finally to a dipole value per cell of 1.57 D for the *cis* form and 1.12 D for the *trans* form, thus rationalizing the larger ΔV_{SAM} contribution for the *cis* form.

The shift in the work function ($\Delta_{CT}\Phi = +140$ meV going from *trans* to *cis*) has an opposite sign when compared to the values obtained for the corresponding non-fluorinated azobenzene derivative[5b] ($\Delta_{CT}\Phi = -100$ meV going from *trans* to *cis*). This difference arises from a larger change in the dipole moment of the cell (by about 0.45 D) between the two isomers (1.57 D for *cis* and 1.12 D for *trans*) when the fluorine substitution is present; the corresponding values are 3.10 and 2.95 D for the *cis* and *trans* forms for the non-fluorinated analogue. This translates into a positive $\Delta_{CT}V_{SAM}$ value (0.27 eV) larger in absolute value than the negative Δ_{CT}BD contribution (−0.13 eV), in contrast to the fully hydrogenated derivative where the negative Δ_{CT}BD term (−0.17 eV) dominates over $\Delta_{CT}V_{SAM}$ (0.07 eV), thus explaining the sign difference in $\Delta\Phi$. On the other hand, a work function shift with the same sign ($\Delta_{CT}\Phi = +220$ meV), with a positive $\Delta_{CT}V_{SAM}$ value (0.13 eV) larger than the Δ_{CT}BD contribution (0.09 eV), has been calculated and measured for another azobenzene derivative with a single phenylene ring in the lower part of the molecule compared to **1**,[5c] thus confirming the role played by the dipole moment associated to the external fluorinated ring.

3.2 Isomerisation in solution

Fig. 1(c) shows the absorption spectrum of **1** in solution with a peak at ~350 nm characteristic of the azobenzene group in its *trans* form. Upon irradiation with UV light ($\lambda = 366$ nm), this peak diminishes and reaches a minimum after 80 s of irradiation. At the same time a smaller peak characteristic of the *cis* form emerges in the visible (~450 nm). Fig. 1d confirms that the back isomerisation (*cis* to *trans*) can be achieved by broadband white light illumination for 50 s. The thermal back isomerisation at 4 °C is much slower with the absorption spectrum after 24 h still closely resembling that of the *cis* isomer.

3.3 Work function measured with ambient photoelectron spectroscopy

Initially, in order to determine the shift in work function (Φ) upon formation of the chemisorbed SAM of **1**, we measured the Φ of pristine Au electrode by ambient photoelectron spectroscopy: Φ_{Au} amounted to 5.08 ± 0.02 eV. Such a value was extracted from the minimum threshold energy beyond which the emission of photoexcited electrons occurs from the ground state. Φ was then measured for both the *trans* and *cis* SAMs formed *ex situ*. This yielded work function values of $\Phi_{trans\text{-}\mathbf{1}/Au} = 5.28 \pm 0.01$ eV and $\Phi_{cis\text{-}\mathbf{1}/Au} = 4.99 \pm 0.08$ eV (Fig. 5).

$\Delta\Phi_{CT}$, defined as the difference between $\Phi_{trans\text{-}\mathbf{1}/Au}$ and $\Phi_{cis\text{-}\mathbf{1}/Au}$ amounts to +290 ± 80 meV and has thus the same sign as predicted by the modelling, though larger in magnitude. In fact, this work function switch is more than double that observed for analogous compounds with a monophenyl bridge separating the sulphur atom from the azo group.[5c] Attempts to monitor the different work function in an *in situ* experiment starting from the *trans* and irradiating the surface with UV light while measuring by photoelectron spectroscopy were unsuccessful most likely because the very same wavelengths used to record a photoelectron spectroscopy spectrum are also needed to activate the *trans* to *cis* isomerization.

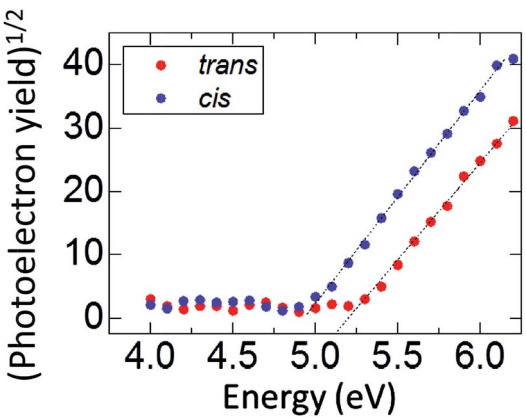

Fig. 5 Square root of photoelectron emission yield as a function of scan energy for **1** SAMs in *trans* and *cis* forms on Au/mica substrate. The dotted lines are linear fits from which the baseline intercept gives the work function of the Au-SAM.

3.4 Contact angle measurement

Differences in surface energy between *cis* and *trans* SAMs of **1** on gold, were sought by measurement of the water contact angle, θ_c, of *ex situ* prepared SAMs, obtaining values of $\theta_{c,cis} = 89 \pm 2°$ and $\theta_{c,trans} = 84 \pm 4°$, and suggesting that the surface energy is not affected by the isomerisation within the accuracy of our measurement. This is not in fact unreasonable when considering that the optimised simulated geometry of the *cis* isomer in the SAM (Fig. 2b) shows a larger opening angle than in the gas phase molecule (119°/124° for the SAM, 86° for gas phase, Fig. 2b). The consequence is that the fluorine atoms are not completely hidden in the *cis* SAM, thereby limiting the change in the surface energy as compared to the *trans* SAM.

3.5 Work function as measured by KP

The surface modification due to UV light as well as the time-evolution after irradiation has been measured with the macroscopic Kelvin Probe (KP) technique. We measured the work function of the freshly prepared *trans* SAM on Au(111) averaged on the scale of mm^2 and how this changes by exposing the monolayer to UV light for 20 minutes, thereby photochemically inducing the transition from *trans* to *cis in situ*. The latter isomeric SAM film was then stored at room temperature in the dark for 21 hours, to allow occurrence of the thermal relaxation *cis* → *trans*.[5b] During such a relaxation, the evolution of the SAM work function was measured as a function of time (Fig. 6).

In freshly irradiated samples the Φ values measured on *cis* and *trans* SAM amount to 5.15 ± 0.02 eV and 5.34 ± 0.02 eV, respectively, with a corresponding difference between the two isomers of $\Delta\Phi_{CT} = 190$ meV. This value is in good quantitative agreement with the value provided by the calculations and measured by ambient photoemission spectroscopy. The reversible switching (*cis* → *trans*) when keeping the sample under dark is monitored by KP, the acquired time-evolution of $\Delta\Phi_{CT}$ being displayed in Fig. 6. It reveals that after 1260 min (*i.e.* 21 hours) the $\Delta\Phi_{CT}$ dropped to about 140 mV. This is due to the positive shift of the *cis* SAM work function tending to the work function value of the *trans* SAM (*i.e.* $\Phi_{cis} \rightarrow \Phi_{trans}$), while the Φ of the *trans* SAM was found being stable over time when stored at room temperature in the dark. The trend of the measured data is fitted with a sigmoidal curve by setting the asymptotic work function difference to zero ($\lim_{t\to\infty} \Delta_{CT}\Phi(t) = 0$). The fitted curve agrees with the experimental data suggesting that the complete reverse switching should be completed after more than 40 hours.

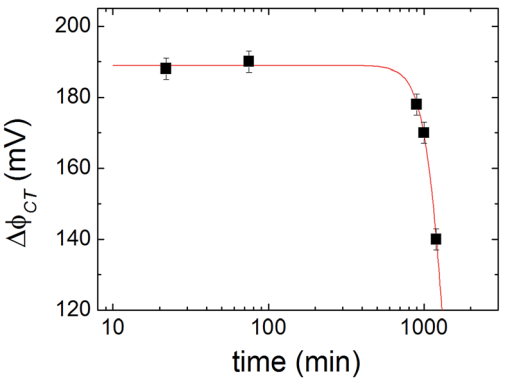

Fig. 6 Work function difference between *trans* and *cis* SAMs on Au as measured by macroscopic KP.

3.6 Work function difference as measured by KPFM

The SAM work function modification has been also monitored by KPFM. As reported by Crivillers *et al.*,[5b] the molecular thermal relaxation occurs in stages and is subordinated to the relaxation of the nearest neighbour in the 2D arrangement. Since the contrast in KPFM images appeared homogeneous on the length scale of tens of nm^2, our measurements offer an average value of the work function in the recorded area (5×5 μm^2).

Two different sample preparation and photoinduced isomerisation approaches have been pursued, *i.e. ex situ* and *in situ* as sketched in Fig. 7.

In the *ex situ* experiment, the chemisorption under visible light led to the formation of *trans* SAMs which exhibited a work function of $\Phi_{trans(ex)} = 4.98 \pm 0.01$ eV. Conversely, *cis* SAMs were produced by first irradiating the solution with UV light for 120 s, then dipping the Au(111) substrate for 24 hours at room temperature under UV illumination. The obtained SAM showed a $\Phi_{cis(ex)}$ of 4.75 ± 0.02 eV, therefore leading to a $\Delta\Phi_{CT(ex)} = 230 \pm 14$ meV, in agreement with the value estimated theoretically. This result confirms the efficient isomerisation from *trans* to *cis*. By storing the sample in dark for 48 hours, the measured Φ raised up to 4.95 ± 0.03 eV, thereby approaching the value measured on *trans*-SAM.

A similar behaviour was observed in the *in situ* experiment. In the as-prepared sample the Φ amounted to $\Delta\Phi_{trans(in)}$ 4.85 ± 0.02 eV. Upon illumination of the SAM with UV light for 20 minutes, thereby photochemically triggering the isomerisation from *trans* to *cis*, the work function exhibited a negative shift, reaching values of $\Delta\Phi_{cis(in)} = 4.63 \pm 0.01$ eV. A successive illumination of the SAM with white light led to a further increase of the Φ up to 4.81 ± 0.02 eV, thus close to the pristine value. One can therefore estimate the $\Delta\Phi_{CT(in)}$ as 220 ± 20 meV, in very good agreement with the *ex situ* result. These comparable *in situ* and *ex situ* values of $\Delta\Phi_{CT}$ suggest a high photoisomerisation quantum yield. Our previous experiments on analogues with a monophenyl bridge between the sulphur atom and the azobenzene group had a lower *in situ* work function switch than was measured for the *ex situ* case or predicted by quantum-chemical calculations. This suggests an increase in photoisomerisation quantum yield going from a monophenyl to biphenyl bridge that would originate from a reduced electrode quenching of the *trans* isomer excited state[9] induced by a weaker electronic coupling to the electrode, as reflected by the reduced bond dipole of the *trans* form (+0.74 eV for the monophenyl bridge, +0.53 eV for the biphenyl bridge). In order to remove all possible contributions of solvent contamination, KPFM measurements were performed on fresh gold substrate immersed in a $CHCl_3$ solution for 24 hours in dark. The measured value amounts to 4.78 ± 0.01 eV in good agreement with Kim *et al.*[22]

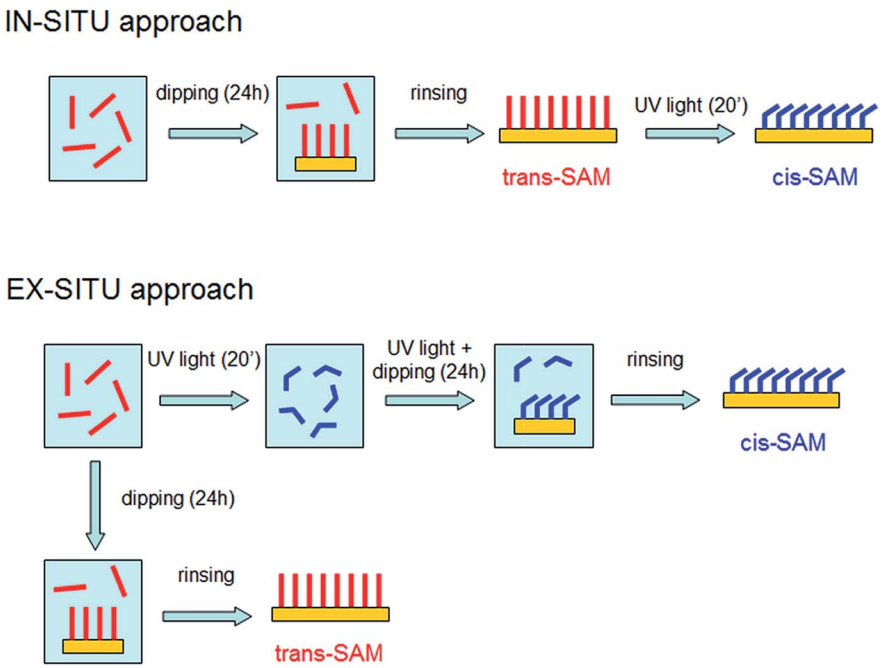

Fig. 7 Cartoon of *in situ* and *ex situ* sample preparation for KPFM measurements.

4. Conclusions

We have designed a biphenyl azobenzene **1** that could undergo *in situ* reversible photochemical isomerisation between a *trans* and a *cis* form directly on the surface of Au(111). In light of the chemical design, such isomerisation was accompanied by a significant change in the work function. Such a property was explored using a wide palette of experimental techniques including ambient photoelectron spectroscopy, macroscopic KP and KPFM, and was further corroborated by quantum-chemical calculations. Ambient photoelectron spectroscopy displayed a value $\Delta\Phi_{CT} = 290$ meV. Macroscopic KP and KPFM showed work function difference between the **1** SAMs in *trans* and *cis* isomeric forms of 190 meV and 220 meV, respectively. The work function difference of the *trans* SAM compared to the *cis* is in close agreement to the value obtained from quantum-chemical calculations, *i.e.* $\Delta\Phi_{CT} = 140$ meV. In all cases the work function of the *trans* SAM was found to be larger than the one of the *cis* SAM, in consistency with our previous report on *cis* and *trans* SAMs on Au based on a similar perfluoro azobenzene embedding a shorter (*i.e.* phenyl) spacer between the anchoring group and the azo moiety. Comparable work function modulation between the *ex-* and *in situ* experiments along with the quantum-chemical calculations suggests a high quantum yield of photoisomerisation *in situ*. In previous work using monophenyl bridging units, *in situ* switching yielded lower work function modulation than predicted by quantum-chemical calculations, suggesting that by using a biphenyl bridging unit we have significantly reduced the quenching of *in situ* photoisomerisation and consequently increased photoisomerisation quantum yields. The minor deviation of the recorded values across different methods is attributed to the inherent contrast in the modes of characterization itself along with the varied operating conditions.

Acknowledgements

This work was financially supported by EC through the Marie-Curie ITN SUPERIOR (PITN-GA-2009-238177) and IEF MULTITUDES (PIEF-GA-2012-326666), the ERC project SUPRAFUNCTION (GA-257305), the Agence Nationale de la Recherche through the LabEx project Chemistry of Complex Systems (ANR-10-LABX-0026_CSC), and the International Center for Frontier Research in Chemistry (icFRC). The work in Mons is further supported by the Interuniversity Attraction Poles Programme (P7/05) initiated by the Belgian Science Policy Office, and by the Belgian National Fund for Scientific Research (FNRS). J.C. is an FNRS research director. The synthesis team in Switzerland acknowledges financial support by the Swiss National Science Foundation (SNF) and the Swiss Nanoscience Institute (SNI).

Notes and references

1 M. M. Russew and S. Hecht, *Adv. Mater.*, 2010, **22**, 3348–3360.
2 (*a*) J. Griffiths, *Chem. Soc. Rev.*, 1972, **1**, 481–493; (*b*) T. Ikeda and O. Tsutsumi, *Science*, 1995, **268**, 1873–1875; (*c*) Z. Sekkat, J. Wood and W. Knoll, *J. Phys. Chem.*, 1995, **99**, 17226–17234; (*d*) N. Tamai and H. Miyasaka, *Chem. Rev.*, 2000, **100**, 1875–1890.
3 (*a*) G. Pace, V. Ferri, C. Grave, M. Elbing, C. von Haenisch, M. Zharnikov, M. Mayor, M. A. Rampi and P. Samorì, *Proc. Natl. Acad. Sci. U. S. A.*, 2007, **104**, 9937–9942; (*b*) M. Elbing, A. Blaszczyk, C. von Haenisch, M. Mayor, V. Ferri, C. Grave, M. A. Rampi, G. Pace, P. Samorì,

A. Shaporenko and M. Zharnikov, *Adv. Funct. Mater.*, 2008, **18**, 2972–2983.
4 E. Orgiu and P. Samorì, *Adv. Mater.*, 2014, **26**, 1827–1845.
5 (*a*) L. F. N. Ah Qune, H. Akiyama, T. Nagahiro, K. Tamada and A. T. S. Wee, *Appl. Phys. Lett.*, 2008, **93**, 083109; (*b*) N. Crivillers, A. Liscio, F. Di Stasio, C. Van Dyck, S. Osella, D. Cornil, S. Mian, G. M. Lazzerini, O. Fenwick, E. Orgiu, F. Reinders, S. Braun, M. Fahlman, M. Mayor, J. Cornil, V. Palermo, F. Cacialli and P. Samori, *Phys. Chem. Chem. Phys.*, 2011, **13**, 14302–14310; (*c*) N. Crivillers, S. Osella, C. Van Dyck, G. M. Lazzerini, D. Cornil, A. Liscio, F. Di Stasio, S. Mian, O. Fenwick, F. Reinders, M. Neuburger, E. Treossi, M. Mayor, V. Palermo, F. Cacialli, J. Cornil and P. Samori, *Adv. Mater.*, 2013, **25**, 432–436; (*d*) T. Nagahiro, H. Akiyama, M. Hara and K. Tamada, *J. Electron Spectrosc. Relat. Phenom.*, 2009, **172**, 128–133.
6 (*a*) V. Ferri, M. Elbing, G. Pace, M. D. Dickey, M. Zharnikov, P. Samori, M. Mayor and M. A. Rampi, *Angew. Chem., Int. Ed.*, 2008, **47**, 3407–3409; (*b*) J. M. Mativetsky, G. Pace, M. Elbing, M. A. Rampi, M. Mayor and P. Samori, *J. Am. Chem. Soc.*, 2008, **130**, 9192–9193.
7 (*a*) M. Han, T. Honda, D. Ishikawa, E. Ito, M. Hara and Y. Norikane, *J. Mater. Chem.*, 2011, **21**, 4696–4702; (*b*) L. M. Siewierski, W. J. Brittain, S. Petrash and M. D. Foster, *Langmuir*, 1996, **12**, 5838–5844; (*c*) S. Sortino, S. Petralia, S. Conoci and S. Di Bella, *J. Mater. Chem.*, 2004, **14**, 811–813.
8 N. Crivillers, E. Orgiu, F. Reinders, M. Mayor and P. Samori, *Adv. Mater.*, 2011, **23**, 1447–1452.
9 (*a*) R. Klajn, *Pure Appl. Chem.*, 2010, **82**, 2247–2279; (*b*) K. Smaali, S. Lenfant, S. Karpe, M. Ocafrain, P. Blanchard, D. Deresmes, S. Godey, A. Rochefort, J. Roncali and D. Vuillaume, *ACS Nano*, 2010, **4**, 2411–2421.
10 (*a*) Y. Jeong, J. W. Han, N. Kim, Y. Lee, C. Lee, M. Hara and J. Noh, *Bull. Korean Chem. Soc.*, 2007, **28**, 2445–2448; (*b*) Y. K. Kang, D. J. Won, S. R. Kim, K. J. Seo, H. S. Choi, G. H. Lee, Z. S. Noh, T. S. Lee and C. J. Lee, *Mater. Sci. Eng., C*, 2004, **24**, 43–46; (*c*) J. M. Tour, L. Jones, D. L. Pearson, J. J. S. Lamba, T. P. Burgin, G. M. Whitesides, D. L. Allara, A. N. Parikh and S. V. Atre, *J. Am. Chem. Soc.*, 1995, **117**, 9529–9534.
11 M. I. Béthencourt, L.-o. Srisombat, P. Chinwangso and T. R. Lee, *Langmuir*, 2009, **25**, 1265–1271.
12 W. N. Hansen and G. J. Hansen, *Surf. Sci.*, 2001, **481**, 172–184.
13 A. Liscio, V. Palermo and P. Samorí, *Acc. Chem. Res.*, 2010, **43**, 541–550.
14 D. R. Lide, *CRC handbook of chemistry and physics: a ready-reference book of chemical and physical data: 2007-2008*, CRC Press, Boca Raton, London, New York, 2008.
15 (*a*) E. Artacho, E. Anglada, O. Dieguez, J. D. Gale, A. Garcia, J. Junquera, R. M. Martin, P. Ordejon, J. M. Pruneda, D. Sanchez-Portal and J. M. Soler, *J. Phys.: Condens. Matter*, 2008, **20**, 064208; (*b*) D. Sánchez-Portal, P. Ordejón, E. Artacho and J. M. Soler, *Int. J. Quantum Chem.*, 1997, **65**, 453–461.
16 (*a*) D. Ceperley, *Phys. Rev. B: Condens. Matter Mater. Phys.*, 1978, **18**, 3126–3138; (*b*) D. M. Ceperley and B. J. Alder, *Phys. Rev. Lett.*, 1980, **45**, 566–569; (*c*) P. A. M. Dirac, *Math. Proc. Cambridge Philos. Soc.*, 1930, **26**, 376–385.
17 H. J. Monkhorst and J. D. Pack, *Phys. Rev. B: Condens. Matter Mater. Phys.*, 1976, **13**, 5188–5192.
18 G. Heimel, L. Romaner, J. L. Brédas and E. Zojer, *Phys. Rev. Lett.*, 2006, **96**, 196806.
19 L. Wang, G. M. Rangger, Z. Ma, Q. Li, Z. Shuai, E. Zojer and G. Heimel, *Phys. Chem. Chem. Phys.*, 2010, **12**, 4287–4290.
20 D. Cornil and J. Cornil, *J. Electron Spectrosc. Relat. Phenom.*, 2013, **189**, 32–38.
21 D. Cornil, Y. Olivier, V. Geskin and J. Cornil, *Adv. Funct. Mater.*, 2007, **17**, 1143–1148.
22 D. K. Kim, T. R. Vemulkar, S. J. Oh, W.-K. Koh, C. B. Murray and C. R. Kagan, *ACS Nano*, 2011, **5**, 3230–3236.